IEEE Access
Multidisciplinary | Rapid Review | Open Access Journal

Received 26 April 2024, accepted 24 June 2024, date of publication 4 July 2024, date of current version 29 July 2024.

Digital Object Identifier 10.1109/ACCESS.2024.3423349

RESEARCH ARTICLE

Enhancing Coastal Air Navigation: eLoran 3-D Positioning and Cycle Slip Mitigation

PYO-WOONG SON[1,2], (Member, IEEE), AND TAE HYUN FANG[1], (Member, IEEE)
[1]Korea Research Institute of Ships and Ocean Engineering, Daejeon 34103, South Korea
[2]Department of Ship and Ocean Engineering Major, University of Science and Technology, Daejeon 34113, South Korea

Corresponding author: Pyo-Woong Son (pwson@kriso.re.kr)

This work was supported in part by Korea Institute of Marine Science and Technology Promotion (KIMST) through the Ministry of Oceans and Fisheries under Grant RS-2023-00256122; in part by Korea Research Institute of Ships and Ocean Engineering Endowment Project "Development of Vertical Positioning Algorithm of eLoran System" through the Ministry of Oceans and Fisheries, South Korea, under Grant 1525014889; and in part by Korea Institute of Marine Science and Technology Promotion (KIMST) through the Ministry of Oceans and Fisheries under Grant RS-2024-00407003.

ABSTRACT The rapid expansion of Advanced Air Mobility has highlighted its significant dependence on Global Navigation Satellite Systems, particularly in the maritime context. This study introduces a novel adaptation of the eLoran system, which, while traditionally utilized for 2D positioning via ground-based radio frequency signals, is now being enhanced to enable 3D position estimation. A key innovation is the development of a 3D positioning method employing a geomatrix and distance calculations specifically designed for non-line-of-sight signals, facilitating eLoran's application in aviation and providing continuous position estimation at various elevations. In addition, this study addresses the challenge of cycle slips in aviation, which is common in dynamic flight conditions. It proposes an algorithm that considers the uncertainty of multiple error sources to effectively mitigate such problems. This approach significantly improves positional accuracy by precisely detecting and correcting cycle slips, ensuring consistent and reliable navigation in rapidly changing flight dynamics. The performance of this advanced eLoran positioning algorithm was evaluated against that of traditional commercial receivers through real-flight experiments. The findings illustrate substantial enhancements in the accuracy and reliability of the eLoran system, offering a dependable navigation alternative that lessens reliance on Global Navigation Satellite Systems and boosts safety and efficiency in maritime and coastal air travel.

INDEX TERMS Advanced air mobility, alternative navigation system, eLoran, terrestrial navigation system.

I. INTRODUCTION

Rapid advancements in smart mobility technologies have emphasized the critical need for accurate and reliable positioning. The Global Navigation Satellite System (GNSS) plays a vital role in offering global positioning support that is widely used in autonomous vehicles, unmanned ships, and aircraft [1], [2], [3]. These systems heavily rely on GNSS for route planning and autonomous navigation. However, the GNSS has limitations, primarily owing to its weak signals from distant satellites and vulnerability to signal disruptions [4], [5].

To overcome these challenges, various auxiliary sensors, such as LiDAR, radar, sonar, and cameras, are used alongside GNSS to help in detecting the surroundings and adjusting the position of the vehicle, especially when GNSS signals are weak or unavailable [6], [7], [8]. Inertial Navigation Systems have been combined with GNSS to provide continuous navigation data. Despite these efforts, the combined use of GNSS and other technologies poses challenges, particularly over long periods without a GNSS. This has led to a growing need for new navigation services based on resilient radio frequency (RF) signals [9].

To further enhance GNSS reliability, multiple GNSS systems, including GPS, GLONASS, Galileo, and BeiDou, have been integrated to significantly improve signal robustness and positioning accuracy by leveraging a diverse array of

The associate editor coordinating the review of this manuscript and approving it for publication was Venkata Ratnam Devanaboyina.

satellites from different constellations, each utilizing distinct signal structures and frequencies, thereby providing a more resilient solution to interference and signal loss [10]. Additionally, Satellite-based Augmentation Systems (SBAS) significantly enhance the accuracy and reliability of GNSS by transmitting corrections through geostationary satellites, which is a crucial feature for high-precision applications, such as aircraft landing procedures [11]. The SBAS achieves this by providing supplementary information to rectify GNSS signal errors caused by ionospheric disturbances, timing discrepancies, and inaccuracies in satellite orbits, thereby ensuring a marked improvement in navigational accuracy [12].

An advanced layer of security in GNSS systems is introduced by Navigation Message Authentication (NMA), as exemplified by the European Union's implementation of open-service NMA [13]. NMA significantly reduces the risk of spoofing attacks by utilizing digital signatures to authenticate GNSS signals where false signals mislead receivers [14]. This system is designed to ensure the integrity of navigation data, making it more difficult for unauthorized sources to corrupt or manipulate signal information. As part of the Galileo satellite system, it serves as a pioneering example of technology that offers publicly accessible signal authentication [15]. This approach enhances the trustworthiness of the GNSS data, which is particularly critical for applications where accuracy and security are paramount, such as aviation, maritime navigation, and critical infrastructure management.

Despite these advancements in GNSS technology and its augmentation, navigational systems that can provide absolute positional coordinates based on high-power RF signals have been increasingly desired [16], [17]. Therefore, the eLoran system has emerged as a viable alternative. eLoran, an evolution of the previously utilized Loran-C system, uses high-power terrestrial signals at 100 kHz. This system is recognized for its robustness against the limitations of satellite-based systems, offering a resilient solution, particularly in environments where satellite signals are obstructed or jammed [18].

South Korea has been proactive in developing an eLoran system in response to the emerging demands [19], [20]. This initiative was motivated by the country's unique political situation with North Korea, which has led to numerous instances of intentional signal disruptions. Historically, these disruptions have affected a multitude of sea vessels and aircraft in the Yellow Sea, underscoring the need for a more resilient navigational system [21]. South Korea currently operates three eLoran transmitters, located on Socheong Island, Pohang, and Gwangju. Expectantly, plans are in place to further expand eLoran services by establishing additional transmitters on Ulleung and Jeju Islands. This expansion aims to extend the eLoran service across all maritime areas, significantly bolstering the nation's capability to provide robust navigational support, particularly in scenarios where conventional GNSS services are compromised.

China is also actively expanding its eLoran system, operating several Loran-C transmission stations along its eastern coastline, configured into three Group Repetition Intervals (GRI). Alongside these coastal Loran-C stations, China operates separate inland transmitters dedicated to time synchronization services, showcasing a comprehensive approach to national navigation and timing infrastructure. Recent scholarly articles have expressed China's ambition to extend eLoran-based time synchronization services across the country by utilizing additional transmission stations [22]. This endeavor is supported by various research efforts focusing on efficient eLoran signal transmission through optimized antenna designs [23], advanced signal processing techniques for precise Time of Arrival (TOA) estimation [24], and correction data application to improve location accuracy [25]. These studies demonstrate a concerted effort to enhance the capabilities of the eLoran system, reflecting a global trend towards more resilient navigational and timing solutions.

Although the use of eLoran systems is expanding internationally to support a growing number of smart mobility solutions, their application in aviation has historically faced limitations owing to their design of providing 2D positioning based on ground waves. However, the rapid evolution of aviation mobility technologies such as Urban Air Mobility and Advanced Air Mobility (AAM) has increased the demand for the incorporation of eLoran in aerial navigation. This need is particularly acute in coastal areas, where the availability of landmarks essential for conventional localization technologies is limited, making GNSS usage challenging, thereby highlighting the potential significance of eLoran for reliable and efficient navigation in such environments.

This study aims to bridge this gap by developing a receiver algorithm that enables existing eLoran systems to provide 3D position data. We focus on adapting eLoran for aerial applications and presenting it as a viable alternative to GNSS, particularly in regions where GNSS reliability is compromised. We first propose a geomatrix and distance calculation that utilizes non-line-of-sight (NLOS) signals, and then develop a cycle confidence algorithm that considers the uncertainty of multiple error sources to mitigate the problems caused by cycle slips, which are common in aerial mobility owing to high speeds and dynamic attitude changes, unlike at sea. To verify the performance of the proposed algorithm, flight experiments were conducted at altitudes used in the AAM corridors. The results demonstrate improved availability and accuracy compared with existing commercial receivers.

II. HISTORICAL DEVELOPMENT AND FUTURE PLAN OF THE KOREAN eLORAN SYSTEM

A. MOTIVATION AND CURRENT STATUS

From 2010 to 2022, South Korea has officially reported six instances of GPS jamming attacks from North Korea that impacted various sectors, including maritime, communication, and aviation. Considering unpublicized military instances, the actual frequency of these disruptions is likely to be higher. These unique circumstances have motivated the South Korean government to develop a stable

and independent navigation system. From 2016 to 2020, South Korea undertook the development of eLoran technology, establishing time synchronization systems at existing Pohang and Gwangju transmission stations and constructing a new low-power (800 W) transmitter for the Incheon testbed, forming a unique GRI 9930 chain [21].

In 2023, the Incheon testbed low-power transmitter was relocated to Socheong Island in the northern Yellow Sea and equipped with an antenna, boosting its effective radiative power to approximately 8 kW. This has made Socheong Island the only station worldwide to simultaneously transmit medium-frequency differential GNSS and eLoran. Additionally, Gwangju station, initially acquired from the U.S. military, was upgraded with an eLoran transmitter developed locally during the eLoran R&D project, which transformed it into a powerful 25 kW eLoran transmitting station.

Currently, South Korea's eLoran system comprises three transmission stations: Pohang station, with an effective radiated power of 150 kW, Gwangju station (25 kW), and Socheong Island station (8 kW). Additionally, the system provides differential Loran correction information services through two differential Loran stations located at the Incheon and Pyeongtaek ports. The correction message was transmitted via the Loran Data Channel (LDC) from the Socheong Island transmission station, further enhancing the accuracy and reliability of the eLoran system in the region.

B. INITIAL OPERATION CAPABILITY AND RESULT

Prior to relocating the low-power eLoran transmitter from the Incheon testbed to Socheong Island, South Korea sought to assess the initial operational capabilities of its eLoran service at the Incheon and Pyeongtaek ports [26]. The accuracy of the eLoran service was evaluated through simulations, as shown in Fig. 1, which illustrates the results derived from the simulations predicting the eLoran service performance, particularly in terms of repeatable positioning accuracy.

A 2021 study demonstrated the capability of the eLoran signal from the Incheon testbed transmitter to provide time synchronization services at Pyeongtaek port. This was achieved with an accuracy of 44 ns (RMS) without any correction information [27]. Furthermore, when the differential Loran correction based on the zero-baseline measurement was applied, the time synchronization accuracy improved to 23 ns (RMS), demonstrating the effectiveness of the correction process in enhancing accuracy. In another study from 2022, the reception rates of differential correction messages were compared using both the Eurofix and 9th Pulse Position Modulation methods [28]. The findings from tests conducted at the Incheon and Pyeongtaek ports revealed that the Eurofix method was more effective in reliably delivering LDC messages to users positioned at greater distances from the transmission stations. Finally, a study published in 2023 examined Korea's eLoran service performance near Incheon port and compared it with that of a Differential GPS receiver installed on a ship [20]. Collectively, these results highlighted the promising capabilities and applications of the eLoran system in South Korea.

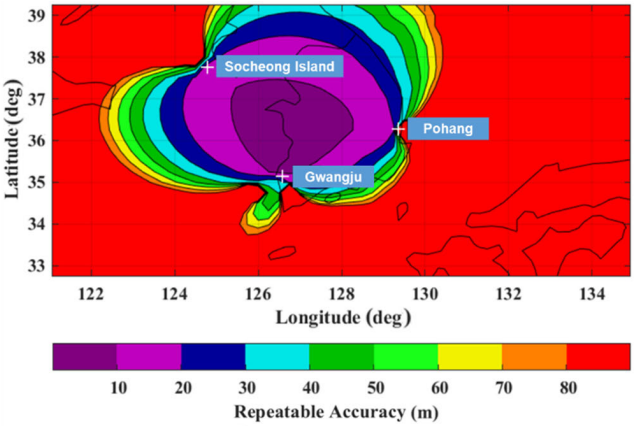

FIGURE 1. Repeatable accuracy simulation result based on the current eLoran system configuration of south korea.

C. FUTURE PLAN

South Korea is set to initiate a new R&D project in 2024 to expand its eLoran services nationwide. The first step involves upgrading the existing Loran-C transmitter in Pohang, which is synchronized with the Universal Coordinated Time (UTC), to an eLoran station capable of transmitting LDC messages. In addition, there are plans to establish eLoran signal monitoring systems across various locations in the country. The data obtained from these systems can be utilized to accurately predict Additional Secondary Factors (ASF) across the nation, including maritime regions. This predicted ASF is expected to contribute significantly to the stable navigation of autonomous ships and AAM. Furthermore, at the 2023 IALA Conference, a government official announced plans to construct additional eLoran transmission stations on Ulleung and Jeju Islands. This expansion aims to extend eLoran services to the South Sea and East Sea regions, thus enhancing the coverage and reliability of eLoran services in South Korea.

III. METHODOLOGY

A. eLORAN SIGNAL SPECIFICATION

The eLoran signal specifications, having evolved from the Loran-C standards as defined by the U.S. Coast Guard in "COMDTINST M16562.4," are further standardized in the SAE9990 document [29], [30]. According to SAE9990, the defining feature of eLoran signals is their leading edge, which must conform to a specific shape. This shape is mathematically represented by (1):

$$I(t) = A(t-\tau)exp\left[-\frac{2(t-\tau)}{65}\right] sin(0.2\pi t + PC) \quad (1)$$

where $I(t)$represents the intensity of the eLoran signal. The normalization constant A correlates with the peak antenna current in amperes, ensuring that the strength of the signal is appropriately scaled. The time variable t is measured in microseconds (μs), and τ, the envelope-to-cycle difference,

represents the time difference between the envelope and the cycle of the signal. The phase-code parameter PC adjusts the signal's phase, taking a value of 0 for a positive phase code and π (pi) for a negative phase code. In the eLoran system, phase codes play a critical role in distinguishing between signals from the master and secondary stations. This is achieved by assigning a sequence of eight continuous codes, alternating between $+\pi$ and $-\pi$. These phase codes facilitate correlation operations within the receiver for eLoran pulse trains, aiding in the accurate identification and decoding of signals.

In the operational framework of the eLoran system, a group of three to five transmitters form a network known as a chain [31]. Each transmitter within this chain broadcasts signals based on a meticulously synchronized schedule relative to the Loran time, which is a standardized reference time. The signals are emitted at intervals that are multiples of the GRI, with each transmitter assigned a specific emission delay within these intervals. Furthermore, a point 30 μs after the start of an eLoran pulse signal is designated as the standard zero crossing (SZC), which serves as a reference point for aligning the timing of signals across the network. This careful arrangement between the transmitters helps spread the eLoran signals efficiently, ensuring that the receivers can pinpoint the TOA accurately.

In the context of eLoran receivers, these devices can receive signals from transmitters associated with different GRIs. The receivers follow a specific process to calculate the TOA of the signals. Initially, during the acquisition phase, the receiver identifies the phase code-modulated GRI signal and the specific transmitting station within the GRI network. The received signal is then compared with an internally generated ideal eLoran signal to accurately determine its TOA, which is pivotal for the receiver to estimate the pseudorange, the distance traveled by the signal from the transmitting station to the receiver's location.

In this study, we employed a UN152B receiver, which is currently the only commercially available eLoran receiver that meets the minimum performance standards established by the Radio Technical Commission for Maritime Services Special Committee-127 (RTCM SC-127) [32]. This model was primarily chosen because of its global usage, which allows for an objective evaluation of our research results.

B. PSEUDO-RANGE ESTIMATION

Electromagnetic waves, including eLoran signals, propagate at the speed of light in vacuum. However, real-world conditions differ because the waves traverse the atmosphere rather than a vacuum. This leads to a delay in the propagation time, which is defined as the Primary Factor (PF). Furthermore, eLoran signals designed for long-range navigation often encounter Secondary Factors (SF) due to signals crossing the sea surface [33]. The nature of the terrain and its ground conductivity also contribute to ASFs, influencing the signal velocity and necessitating adjustments to the pseudorange calculations.

The RTCM SC-127 outlines the TOA processing for pseudorange estimation as (2).

$$\rho = TOA * c - p - [ASF + \delta] * 10^{-6} * c \tag{2}$$

where ρ denotes the pseudorange measured (m); TOA is the TOA measured at the receiver (μs); c represents the speed of light; p accounts for the phase delay (m), covering both PF and SF; ASF is the published ASF value at the estimated position (μs); and δ denotes the differential eLoran correction (μs).

Both PF and SF, along with ASF, comprise elements that are constant over time, as well as those that vary. For example, propagation time alterations due to static geographical features, such as terrain, remain steady, whereas changes in sea salinity or atmospheric conditions can cause fluctuations in propagation times [34]. The constant aspects of PF and SF are modelled based on distance, utilizing Brunavs' equation for correction, whereas static ASF values are premeasured and disseminated to users in the form of maps. Conversely, dynamic elements are captured in real-time at differential eLoran stations and transmitted to users via the LDC. By integrating this extensive data, receivers can accurately estimate the pseudorange, thereby accounting for the complexities introduced by NLOS conditions.

C. CYCLE SLIP MITIGATION ALGORITHM

In low signal-to-noise ratio (SNR) environments, an eLoran system operating at a carrier frequency of 100 kHz is particularly vulnerable to cycle detection errors, leading to incorrect identification of the SZC [35]. This vulnerability is pronounced in the aviation sector, particularly within AAM, where the rapid dynamics of aircraft movements and complex signal multipath effects can further degrade the SNR of eLoran signals. Consequently, even a single cycle slip could result in a ranging error of several kilometers.

To address these challenges, various techniques, including the delay-locked loop and matched filter methods, have been explored [36], [37], [38]. Each offers potential solutions under different conditions, albeit with varying success rates. However, these methods often prove inadequate for navigating the intricate dynamics and multipath challenges inherent to signal propagation, leading commercial eLoran receivers to produce TOA measurements contaminated with undetected cycle slips. Therefore, rectifying these inaccuracies is crucial for ensuring accurate and resilient positioning in aviation applications, highlighting the urgent need for advanced methodologies that can effectively mitigate cycle slips.

In the positioning process using TOA data from the eLoran receivers, the detection of cycle slips significantly depends on the presence of redundant signals. Because of sufficient redundancy in eLoran signals, advanced methodologies such as the weighted sum squared error (WSSE) statistic and multiple hypothesis solution separation (MHSS) approach are employed to detect cycle slips [39]. The WSSE technique calculates an error statistic by weighting the sum of

the squared differences between the observed and expected signal characteristics, allowing for the identification of anomalies indicative of cycle slips. In contrast, MHSS utilizes a comparison among multiple possible scenarios, effectively separating correct signal paths from erroneous paths caused by cycle slips.

However, in scenarios where redundancy is unavailable, devising a unique judgment process for each signal is essential. Utilizing TOA data from previous measurements can prove invaluable for detecting undetected cycle slips in the TOAs of eLoran signals. Under the assumption that all external corrections, including ASF and differential eLoran correction, have been implemented, the difference ($\Delta\rho$) between the pseudorange estimated from these prior data points ($\hat{\rho}$) and the currently measured pseudorange (ρ) can be calculated, as shown in (3):

$$\Delta\rho = \hat{\rho} - \rho \sim N(0, \sigma_{total}) \tag{3}$$

This statistical value ideally follows a distribution with a mean of zero and a variance denoted by σ_{total}, which encapsulates the cumulative uncertainties from various sources, including ASF, user dynamics, and pseudorange estimation, as indicated in (4):

$$\sigma_{total} = \sigma_{ASF} + \sigma_{dynamics} + \sigma_{psuedorange} \tag{4}$$

where σ_{ASF} reflects the uncertainty in the ASF correction, $\sigma_{dynamics}$ quantifies the uncertainty in estimating psuedorange based on previous measurements, and σ_{range} signifies the noise in the eLoran TOA pseudorange measurements. Given that cycle slips in eLoran signals occur in increments of 5 μs, the magnitude of undetected cycle slips can be estimated by finding a value of k that satisfies (5).

$$\underset{k}{argmax}\ normcdf\,(\Delta\rho, 5k, \sigma_{total}) \tag{5}$$

If the value of k that satisfies (5) is zero, that no cycle slip has occurred in the current epoch. The proposed method's effectiveness hinges on the assumption that each uncertainty's bias is zero and its magnitude is significantly smaller than the 5 μs increment of a cycle slip occurrence (This is supported by the research conducted by Sherman Lo, 2006). Therefore, caution is advised when applying this technique because it presumes minimal influence from uncertainties relative to the scale of the potential cycle slips.

D. SIGNAL PROPAGATION PATH FOR AIR NAVIGATION

Understanding the propagation path of eLoran signals from ground-based transmitters is essential for the accurate measurement of their distances to user receivers. As depicted in Fig. 2, users may receive these signals in either line-of-sight (LOS) or NLOS mode, depending on their distance from the transmitter and altitude. To calculate the maximum LOS distance (d) from the transmitter, considering atmospheric refraction (K), a modified formula is applied as follows:

$$d = \sqrt{2RKh_t + h_t^2} + \sqrt{2RKh_r + h_r^2} \tag{6}$$

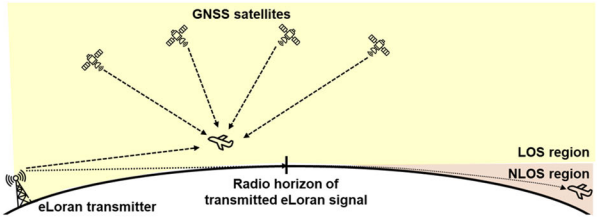

FIGURE 2. LOS and NLOS conditions of the eLoran signal.

In this formula, R is the radius of the Earth, approximately 6371 km; K is the correction factor for atmospheric refraction, commonly set to 4/3 in standard condition; h_t is the height of the transmitting antenna, and h_r is the height of the user receiver with both heights measured (km).

Specifically, the 137 m height of the antenna, matching the actual height of the Pohang transmitter's top-loaded monopole (TLM) antenna, serves as a concrete example. The phase center of a TLM antenna is situated at its peak, and signals transmitted from this height enable users at sea level to receive the signal in LOS from up to approximately 40 km, a distance that corresponds to the Radio Horizon of the transmitted eLoran signal, as illustrated in Fig. 2. AAM vehicles operating at altitudes between 300 and 600 m, particularly at an altitude of 450 m under identical transmission conditions, can achieve LOS signal reception for distances of up to approximately 130 km. Commercial airliners flying at an altitude of approximately 10 km can extend their LOS reception capabilities to approximately 460 km.

This analysis reveals that maritime users typically receive eLoran signals as NLOS signals, whereas aviation users may experience a mix of LOS and NLOS signals, with the variation influenced not only by their distance from the transmission tower but also their altitude. The propagation speed of LOS signals is influenced by atmospheric conditions, whereas that of NLOS signals is affected by the Earth's or marine surface. Consequently, precise distance estimation based on the TOA of eLoran signals requires careful consideration of the travel path of the signal.

E. eLORAN 3D POSITION ESTIMATION

The process of estimating an aviation user's 3D position using LOS signals in the Earth-centered, Earth-fixed coordinate system involves a series of mathematical steps to minimize the error between the measured and actual distances from the signal transmitters. The user position vector is denoted as p:$[x, y, z]^T$ and each signal transmitter's position vector is represented by $\boldsymbol{s_i}$:$[x_i, y_i, z_i]^T$, where i is the index of the signal transmitters. If the initial guess of the user position vector in is $\boldsymbol{p}_0$:$[x_0, y_0, z_0]^T$, then the geometric range vector $\boldsymbol{r_0}$ between the initial guess position and signal transmitters is defined as:

$$\boldsymbol{r_0} = \|\boldsymbol{p_0} - \boldsymbol{s}\| \tag{7}$$

The pseudorange vector $\boldsymbol{\rho}$ obtained from the receiver's TOA measurement consists of geometric range vector $\boldsymbol{r}$ and

receiver clock bias b as:

$$\boldsymbol{\rho} = \boldsymbol{r} + b = \|\boldsymbol{p} - \boldsymbol{s}\| + b \tag{8}$$

The difference between the pseudorange and the geometric range of the initial guess position can be represented as:

$$\boldsymbol{\rho} - (\boldsymbol{r_0} + b_0) = \boldsymbol{G}[\delta \boldsymbol{p} \delta b]^{\boldsymbol{T}} + \boldsymbol{\varepsilon} \tag{9}$$

where,

$$\boldsymbol{G} = [\|\boldsymbol{p_0} - \boldsymbol{s}\|^{-1} (\boldsymbol{p_0} - \boldsymbol{s})\, \boldsymbol{1}_n] \tag{10}$$

$$\delta \boldsymbol{p} = \hat{p} - \boldsymbol{p_0} \tag{11}$$

$$\delta b = \hat{b} - b_0 \tag{12}$$

Matrix $\boldsymbol{G}$ is constructed from the normalized LOS vectors of the user to each transmitter, concatenated with a column of vectors to account for the clock bias. $\boldsymbol{\varepsilon}$ is the combined effect of residual error vector and n is the number of signal transmitter. To minimize the residual error, the derivatives of $\boldsymbol{\varepsilon^2}$ should be set to zero.

$$2\boldsymbol{G}^{\boldsymbol{T}} \boldsymbol{W} \boldsymbol{G}([\delta \boldsymbol{p} \delta b]^{\boldsymbol{T}}) - 2\boldsymbol{G}^{\boldsymbol{T}} \boldsymbol{W}(\boldsymbol{\rho} - (\boldsymbol{r_0} + b_0)) = 0 \tag{13}$$

$$[\widehat{\delta \boldsymbol{p}} \widehat{\delta b}]^{\boldsymbol{T}} = (\boldsymbol{G}^{\boldsymbol{T}} \boldsymbol{W} \boldsymbol{G})^{-1} \boldsymbol{G}^{\boldsymbol{T}} \boldsymbol{W}(\boldsymbol{\rho} - (\boldsymbol{r_0} + b_0)) \tag{14}$$

The weighting matrix $\boldsymbol{W}$, which is inversely proportional to the variance of each pseudorange measurement, prioritizes the more reliable measurements in the estimation process. Finally, the improved estimated position and clock bias are updated as follows:

$$\hat{p} = \hat{\delta \boldsymbol{p}} + \boldsymbol{p_0} \tag{15}$$

$$\hat{b} = \hat{\delta b} + b_0 \tag{16}$$

This iterative process continues until the change in the estimated position and clock bias between iterations falls below a predetermined threshold, indicating convergence to the final solution.

However, eLoran signals can be received in NLOS form, depending on the altitude of the user and the distance to the signal transmitter. In such cases, the method for calculating $\boldsymbol{G}$, which represents the geometric vector between the user's position, the transmitter, and the geometric range $\boldsymbol{r}$, must be adjusted. If the azimuth between the user's position and each ith transmitter's location is denoted as θ^i_{az}, and the elevation angle between the user and ith transmitter is θ^i_{elev}, then modified $\boldsymbol{G'}$ can be designed as follows.

$$\boldsymbol{G'} = \begin{bmatrix} -cos(\theta^1_{elev})sin(\theta^1_{az}) & -cos(\theta^1_{elev})cos(\theta^1_{az}) & -sin(\theta^1_{elev}) & 1 \\ \vdots & & \vdots & \\ -cos(\theta^n_{elev})sin(\theta^n_{az}) & -cos(\theta^n_{elev})cos(\theta^n_{az}) & -sin(\theta^n_{elev}) & 1 \end{bmatrix} \tag{17}$$

Furthermore, the modified geometric range $\boldsymbol{r'}$ incorporates the elevation angle vector $\boldsymbol{\theta_{elev}}$ and the distances vector $\boldsymbol{r_{vincenty}}$ based on the Vincenty algorithm defined as follows.

$$\boldsymbol{r'} \approx (cos\boldsymbol{\theta_{elev}})^{-1} \boldsymbol{r_{vincenty}} \tag{18}$$

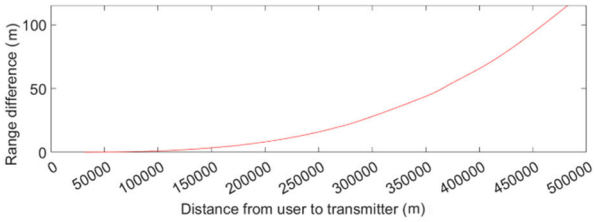

FIGURE 3. Estimated range difference between the traditional method under LOS conditions (Equation 8) and the proposed method under NLOS conditions (Equation 18).

The Vincenty algorithm is well-known for its accuracy in calculating the distances between two geographic locations on the Earth's surface based on the WGS84 model, making it particularly effective for estimating the geometric range of NLOS signals [32]. Assuming that both the transmitter and user are located at sea level or on the ground at an altitude of zero, the difference in distance measurements between the traditional LOS calculation method and the method proposed in this study is illustrated in Fig. 3. At a distance of approximately 350 km from the transmitter, the discrepancy in the measured distances between the two methods was approximately 50 m. This implies that aerial eLoran users who calculate their position using the LOS method may experience discontinuous positional measurement errors of tens of meters near the sea surface at altitudes close to zero.

IV. EXPERIMENTAL SETUP AND ENVIRONMENT

To ensure the validity of the proposed algorithm, an experimental setup that involved data collection aboard a light aircraft equipped with eLoran and GNSS receivers was designed, specifically targeting coastal flight routes. As illustrated in Fig. 4, the setup included the eLoran H-field antenna and receiver, the UN152B model from Ursanav, coupled with Hemisphere's A42 GNSS antenna and Novatel's PwrPak7 GNSS receiver. These devices, which were not originally intended for use in light aircraft, were adapted for temporary installation within aircraft safety guidelines. This setup may have affected the quality of the data collected.

In terms of data output, the eLoran receiver from Ursanav rendered information in the National Marine Electronics Association format, with position details available under the LCPOSA tag, and signal specifics such as signal strength (SS), SNR, and TOA under the TOAA tag. The classification of the eLoran position information output depends on the use of the correction information. This setup permits a direct comparison between the receiver-provided position results and those calculated using the proposed method, facilitating an accurate assessment of the impact of the algorithm on eLoran positioning performance.

The positional accuracy of the proposed algorithm was gauged against the GNSS data from Novatel's TerraStar-C PRO precision positioning solution. This high-precision service, which refines global PPP capabilities to deliver centimeter-level accuracy within minutes, serves as a reliable benchmark for evaluating the effectiveness of the eLoran

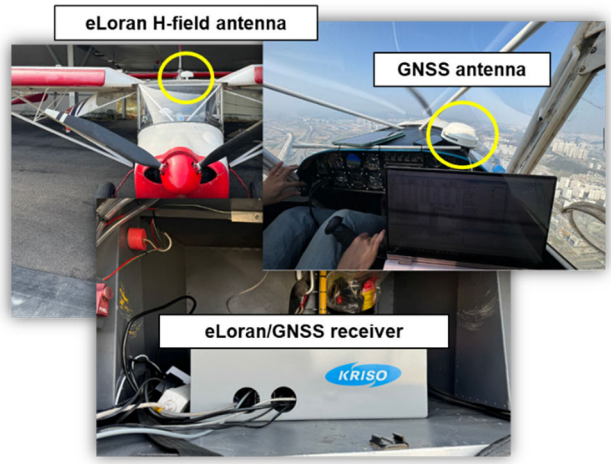

FIGURE 4. Experimental setup of eLoran and GNSS antenna/receiver at the light airplane.

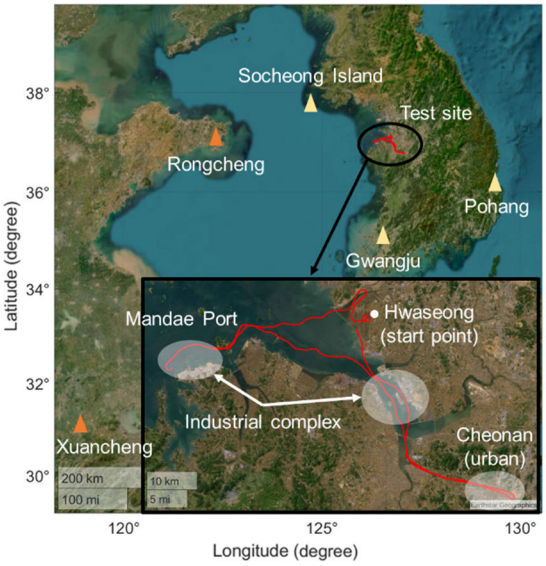

FIGURE 5. Distribution of eLoran transmitters and location of test site. The test site is composed of complex signal propagation from each transmitter.

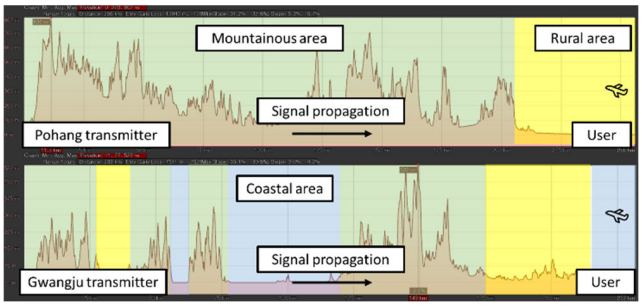

FIGURE 6. Geological features of the signal propagation path from the Pohang and Gwangju transmitters.

system with an accuracy of tens of meters. Utilizing the BESTPOS log data, which indicates the receiver's most accurate calculated position, and looking for the "PPP" indicator in the postype field allowed us to validate the operational success of the TerraStar-C PRO and thereby confirm the eLoran system's performance under diverse conditions.

After configuring our equipment, the chosen flight path, depicted by the red line in Fig. 5, began at Hwaseong, passed through Mandae Port and Cheonan, and returned to the starting point. This circuit covers an approximate distance of 150 km and includes diverse terrains, such as coastal regions, rural and urban areas, and industrial complexes. During flight, the eLoran receiver received signals from five transmission stations—Pohang, Gwanju, Socheong Island, Rongcheng, and Xuancheng—propagating through environments with distinct geological features and path lengths. As illustrated in Fig. 3, the discrepancy between the estimated range using conventional methods under LOS conditions and that of our proposed method increases with the distance from the transmitter. Table 1 presents the distances from the starting point of the experiment to each of the five transmission stations, ensuring that the signal propagation paths were adequately long for a thorough assessment of the performance of our algorithm.

Fig. 6 illustrates the varied geological features along the signal paths from the experimental site's starting point to the Pohang and Gwangju transmission stations. The path from the site to the Pohang station traverses through mountainous regions with peaks up to 607 m, whereas the route to Gwangju station also crosses over areas with high elevation, reaching up to 522 m, alongside diverse landscapes that include rural and coastal areas. The signal paths from Socheong Island, Rongcheng, and Xuancheng stations predominantly cover sea areas and low-lying lands. These different environments at the experimental site provide a comprehensive setting to thoroughly evaluate the effectiveness of the proposed algorithm.

V. RESULTS AND DISCUSSION

Focusing on the evaluation of the effectiveness of the proposed 3D positioning and cycle slip correction algorithm, the analysis commenced with an examination of the SNR measurements of the five eLoran signals from the Ursanav receiver to understand the conditions under which the experimental flights were conducted and their potential impact on the performance of the positioning system. As illustrated in Fig. 7, in addition to the signals from Xuancheng, which maintained the SNR levels to above 0 dB, the SNR of the other signals predominantly remained below this threshold. This indicates that the conditions were not ideal for precise eLoran positioning. However, the generally low SNR can be attributed to factors such as the temporary installation of equipment on a light aircraft and the use of antennas intended for maritime users, which may not have been optimized for aerial reception.

A significant event at approximately 12:05 saw all receivers reboot owing to a temporary power system problem, thereby disrupting signal collection, as both the GNSS and eLoran receivers were in the midst of re-acquiring signals. This event demonstrated that the UN152B receiver takes

TABLE 1. Surface distances from the test site to each transmitter.

Station	GRI	Surface distance (km)
Pohang	9930	255
Gwangju	9930	230
Socheong Island	9930	191
Rongcheng	7430/8390	391
Xuancheng	7430/8390	985

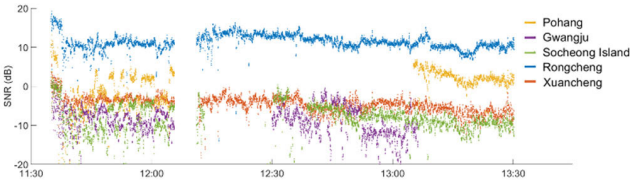

FIGURE 7. SNR of the five eLoran signals during the flight campaign.

approximately 5 min to complete the signal acquisition process, not meeting the RTCM SC-127 requirement for Time to Reacquire Fix, which was set at a maximum of 2 min. In comparison, the TerraStar-C PRO service delivered converged precise positions within approximately 3 min, in line with its specification sheet. Subsequent observations revealed that the signal from Gwangju started to be received around 12:30, approximately 20 min after the reboot, whereas a relatively high SNR signal from Pohang was not detected until around 13:00, as the flight returned through the urban area of Cheonan. This indicates that navigating signals through diverse terrain presents challenges in the signal acquisition phase, regardless of the SNR. Furthermore, reception from Gwangju ceased after 13:10 for reasons that remain undetermined.

The data from the eLoran receiver's TOAA tags was post-processed to assess the accuracy of the final eLoran positioning, depicted by blue dots in Fig. 8, against the reference position obtained from TerraStar-C PRO. One-time calibration employing the reference position from the initial epoch facilitated the estimation of the ASF and delta terms in accordance with (2), providing a foundation for a direct comparison of eLoran positioning accuracy throughout the flight. This calibration process is critical for the accurate evaluation of the performance of the algorithm in the absence of aviation-specific ASF maps or differential correction services.

Fig. 9 shows the horizontal and vertical positioning accuracies of the eLoran system compared with the reference positions based on the data collected during the experiment. The upper part of Fig. 9 illustrates the horizontal positioning accuracy, whereas the lower part details the vertical positioning accuracy. For the horizontal positioning results, the data processed using only the initial calibration are marked with red dots. The results before 12:00 during the coastal flight segments showed relatively minor positioning errors and appeared to contain less noise in the error margin. However, data collected after 12:30 PM during flights near industrial complexes and urban areas exhibited a significant increase in both the bias and noise components within the positioning

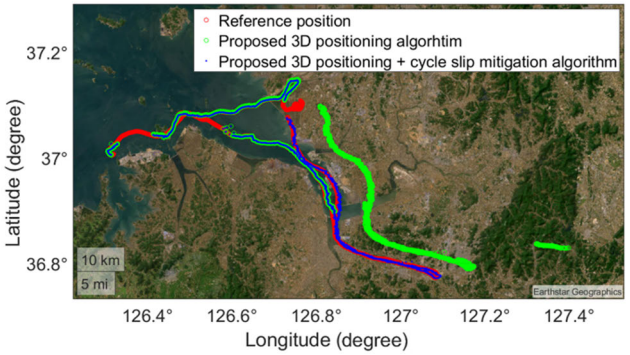

FIGURE 8. eLoran positioning results during the flight campaign. Red circles show the reference position by Terrastar-C PRO and green circles show the eLoran position using the proposed 3D positioning algorithm. Blue dots show the eLoran positioning results with both 3D positioning and cycle slip mitigation algorithms.

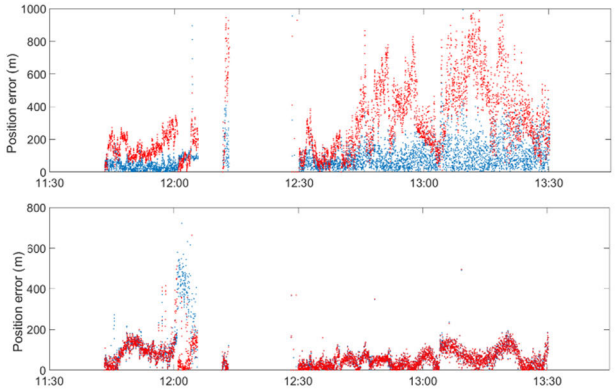

FIGURE 9. eLoran position accuracy over time during the flight campaign (top: horizontal position error, bottom: vertical position error).

error. This reflects the characteristics of terrestrial signals, where the signal delay varies according to the propagation path features. The results depicted by the blue dots in Fig. 9 are achieved using a simplified ASF correction method similar to that used in maritime contexts, which estimates the ASF with each measured data point and smooths it to eliminate bias in the positioning error. As aviation-specific ASF maps are further developed and distributed, we anticipate a horizontal positioning accuracy of approximately 250 m under similar conditions and with the same hardware, as demonstrated by the results represented by blue dots.

For the vertical positioning results, the outcomes before and after applying the estimated ASF showed no significant difference, unlike the horizontal positioning results. This phenomenon is likely due to the experimental conditions, in which low elevation angles (θ_{elev}) caused the influence of the third column in the $\boldsymbol{G}'$ matrix to be negligible, resulting in insignificant adjustments during the iterative process. Vertical positioning appeared more akin to adding noise to the altitude value from the previous position rather than reflecting changes in altitude based on the TOA input values. In scenarios with increased user altitude or reduced distance to the transmission stations, which result in higher elevation angles, the adaptation in TOA attributed to altitude changes

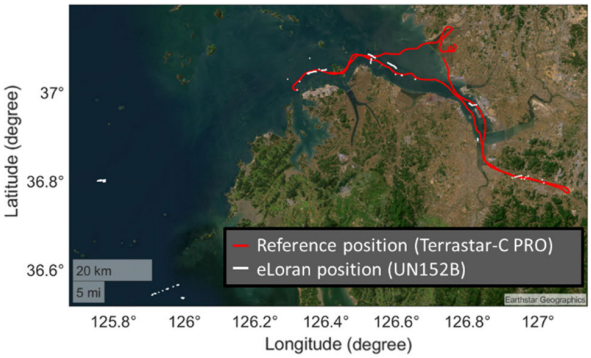

FIGURE 10. Trajectories of reference position and the eLoran position outputted by the commercial eLoran receiver (UN152B).

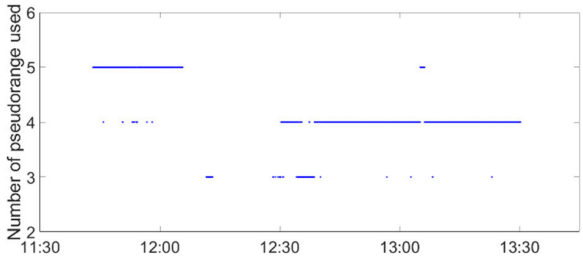

FIGURE 11. The number of pseudorange used during the flight campaign.

is anticipated to be more accurately translated into altitude adjustments.

Beyond accuracy, the proposed algorithm also demonstrated superior availability compared with existing results. The blue dots in Fig. 8 exemplify the effective mitigation of two significant cycle slips, illustrating that out of the 5,051 epochs in which at least three signals were received, positioning was possible for 4,930 epochs. In contrast, as indicated by the white dots in Fig. 10, the most widely used commercial receiver was only able to calculate the positions for 469 epochs, and even these results were unreliable in terms of accuracy. Given that the UN151B receiver is equipped with a positioning algorithm designed for maritime users, this comparative analysis suggests that the proposed algorithm not only improves the accuracy but also enhances the availability of traditional methods. Additionally, Fig. 11 depicts the variation in the number of pseudorange signals utilized for positioning. It is important to note that when the number of pseudorange signals is limited to three, the system lacks redundancy for cycle slip detection based on the traditional methods. Nonetheless, even under these non-redundant conditions, this result demonstrates the robustness and reliability of the proposed positioning algorithm in scenarios with minimal signal availability.

This research has successfully developed an algorithm that can be applied to air navigation using outputs from existing commercial receivers, marking a significant step forward. However, it is worth noting that this study relies on processed results from these receivers, and not directly on the RF raw signals. Utilizing raw signals could potentially allow for the development of even more refined algorithms. Moreover, the location of our algorithm testing was near the geometric network boundary of the transmission stations, which may have influenced the positioning performance. This factor should be considered when analyzing the results. Additionally, if prior knowledge about the variance of signal noise is available, noise reduction could effectively be achieved through methods such as the Kalman filter, potentially leading to improved positioning outcomes. This adds a layer of complexity and opportunity for future research, suggesting that with access to raw signal data and a more central position within the transmitter network, the algorithm's effectiveness and applicability could be significantly enhanced.

VI. CONCLUSION

In this study, we proposed and validated 3D positioning and cycle slip mitigation within the eLoran system to enhance coastal air navigation, especially for AAM. The algorithm was empirically assessed through experimental flights incorporating precise GNSS and eLoran data. The experimental setup, which involved data collection aboard a light aircraft along coastal flight paths, provided significant insights into the operational challenges and limitations of utilizing eLoran for aviation purposes. Despite the obstacles, such as non-aviation-specific antenna designs and temporary equipment installation, the proposed algorithm significantly improved the accuracy and availability of eLoran-based positioning compared with commercial products, which are assumed to utilize traditional methods. This finding indicates the potential for quickly testing the performance of eLoran services for AAM using existing commercial receiver products. The potential development of aviation-specific ASF maps and differential correction services could greatly facilitate the implementation of an independent navigational system service, free from GNSS reliance. To further enhance the performance beyond what was achieved in this study, the addition of more transmission stations and the development of high-performance dedicated receiving hardware may be required. Such advancements could significantly improve the accuracy of eLoran, establishing it as a feasible alternative or complement to GNSS, particularly in scenarios where GNSS signals are compromised or unavailable.

REFERENCES

[1] A. Eskandarian, C. Wu, and C. Sun, "Research advances and challenges of autonomous and connected ground vehicles," *IEEE Trans. Intell. Transp. Syst.*, vol. 22, no. 2, pp. 683–711, Feb. 2021, doi: 10.1109/TITS.2019.2958352.

[2] J. Jung, J. Park, J. Choi, and H.-T. Choi, "Navigation of unmanned surface vehicles using underwater geophysical sensing," *IEEE Access*, vol. 8, pp. 208707–208717, 2020, doi: 10.1109/ACCESS.2020.3038816.

[3] H. Lee, S. Pullen, J. Lee, B. Park, M. Yoon, and J. Seo, "Optimal parameter inflation to enhance the availability of single-frequency GBAS for intelligent air transportation," *IEEE Trans. Intell. Transp. Syst.*, vol. 23, no. 10, pp. 17801–17808, Oct. 2022, doi: 10.1109/TITS.2022.3157138.

[4] J. Lee, Y. T. J. Morton, J. Lee, H.-S. Moon, and J. Seo, "Monitoring and mitigation of ionospheric anomalies for GNSS-based safety critical systems: A review of up-to-date signal processing techniques," *IEEE Signal Process. Mag.*, vol. 34, no. 5, pp. 96–110, Sep. 2017.

[5] A. Grant, P. Williams, N. Ward, and S. Basker, "GPS jamming and the impact on maritime navigation," *J. Navigat.*, vol. 62, no. 2, pp. 173–187, Apr. 2009.

[6] J. H. Rhee and J. Seo, "Low-cost curb detection and localization system using multiple ultrasonic sensors," *Sensors*, vol. 19, no. 6, p. 1389, Mar. 2019, doi: 10.3390/s19061389.

[7] X. Li, H. Wang, S. Li, S. Feng, X. Wang, and J. Liao, "GIL: A tightly coupled GNSS PPP/INS/LiDAR method for precise vehicle navigation," *Satell. Navigat.*, vol. 2, no. 1, p. 26, Dec. 2021, doi: 10.1186/s43020-021-00056-w.

[8] J. Zhu, H. Zhou, Z. Wang, and S. Yang, "Improved multi-sensor fusion positioning system based on GNSS/LiDAR/vision/IMU with semi-tight coupling and graph optimization in GNSS challenging environments," *IEEE Access*, vol. 11, pp. 95711–95723, 2023, doi: 10.1109/ACCESS.2023.3311359.

[9] G. Sadlier, R. Flytkjær, F. Sabri, and D. Herr, "The economic impacton the UK of a disruption to GNSS," London Econ., London, U.K., Tech. Rep., 17.3254, Jun. 2017. [Online]. Available: https://www.gov.uk/government/publications/the-economic-impact-on-the-uk-of-a-disruption-to-gnss

[10] D.-K. Lee, Y. Lee, and B. Park, "Carrier phase residual modeling and fault monitoring using short-baseline double difference and machine learning," *Mathematics*, vol. 11, no. 12, p. 2696, Jun. 2023, doi: 10.3390/math11122696.

[11] H. Yoon, H. Seok, C. Lim, and B. Park, "An online SBAS service to improve drone navigation performance in high-elevation masked areas," *Sensors*, vol. 20, no. 11, p. 3047, May 2020, doi: 10.3390/s20113047.

[12] C. Lim, B. Park, and Y. Yun, "L1 SFMC SBAS message for service expansion of multi-constellation GNSS support," *IEEE Access*, vol. 11, pp. 81690–81710, 2023, doi: 10.1109/ACCESS.2023.3300580.

[13] J. Blanch, T. Walter, and P. Enge, "Position error bound calculation for GNSS using measurement residuals," *IEEE Trans. Aerosp. Electron. Syst.*, vol. 44, no. 3, pp. 977–984, Jul. 2008, doi: 10.1109/TAES.2008.4655357.

[14] B. Motella, M. Nicola, and S. Damy, "Enhanced GNSS authentication based on the joint CHIMERA/OSNMA scheme," *IEEE Access*, vol. 9, pp. 121570–121582, 2021, doi: 10.1109/ACCESS.2021.3107871.

[15] K. Zhang, E. G. Larsson, and P. Papadimitratos, "Protecting GNSS open service navigation message authentication against distance-decreasing attacks," *IEEE Trans. Aerosp. Electron. Syst.*, vol. 58, no. 2, pp. 1224–1240, Apr. 2022, doi: 10.1109/TAES.2021.3122512.

[16] E. Chătre and M. Manteiga, "Galileo programme status," in *Proc. 35th Int. Tech. Meeting Satell. Division The Inst. Navigat.*, Denver, Colorado, Oct. 2022, pp. 484–511, doi: 10.33012/2022.18577.

[17] G. Offermans, S. Bartlett, and C. Schue, "Providing a resilient timing and UTC service using eLoran in the United States," *Navigation*, vol. 64, no. 3, pp. 339–349, Sep. 2017.

[18] P.-W. Son, J. H. Rhee, and J. Seo, "Novel multichain-based Loran positioning algorithm for resilient navigation," *IEEE Trans. Aerosp. Electron. Syst.*, vol. 54, no. 2, pp. 666–679, Apr. 2018.

[19] Y. Li, Y. Hua, B. Yan, and W. Guo, "Research on the eLoran differential timing method," *Sensors*, vol. 20, no. 22, p. 6518, Nov. 2020, doi: 10.3390/s20226518.

[20] P.-W. Son, J. H. Rhee, J. Hwang, and J. Seo, "Universal Kriging for Loran ASF map generation," *IEEE Trans. Aerosp. Electron. Syst.*, vol. 55, no. 4, pp. 1828–1842, Aug. 2019, doi: 10.1109/TAES.2018.2876587.

[21] P.-W. Son, S. G. Park, Y. Han, K. Seo, and T. H. Fang, "Demonstration of the feasibility of the Korean eLoran system as a resilient PNT in a testbed," *Remote Sens.*, vol. 15, no. 14, p. 3586, Jul. 2023, doi: 10.3390/rs15143586.

[22] P.-W. Son, S. G. Park, Y. Han, and K. Seo, "ELoran: Resilient positioning, navigation, and timing infrastructure in maritime areas," *IEEE Access*, vol. 8, pp. 193708–193716, 2020, doi: 10.1109/ACCESS.2020.3033215.

[23] C. Yang, S. Li, and Z. Hu, "Analysis of the development status of eLoran time service system in China," *Appl. Sci.*, vol. 13, no. 23, p. 12703, Nov. 2023, doi: 10.3390/app132312703.

[24] K. Wang, S. Tang, J. Ke, and Y. Hou, "A small active magnetic antenna of Loran-C," *IEEE Sensors J.*, vol. 23, no. 1, pp. 647–657, Jan. 2023, doi: 10.1109/JSEN.2022.3222577.

[25] W. Yan, K. Zhao, S. Li, X. Wang, and Y. Hua, "Precise Loran-C signal acquisition based on envelope delay correlation method," *Sensors*, vol. 20, no. 8, p. 2329, Apr. 2020, doi: 10.3390/s20082329.

[26] B. Yan, Y. Li, W. Guo, and Y. Hua, "High-accuracy positioning based on pseudo-ranges: Integrated difference and performance analysis of the Loran system," *Sensors*, vol. 20, no. 16, p. 4436, Aug. 2020, doi: 10.3390/s20164436.

[27] P. W. Son, T. H. Fang, S. G. Park, Y. Han, and K. Seo, "Compensation method of eLoran signal's propagation delay and performance assessment in the field experiment," *J. Positioning, Navigat., Timing*, vol. 11, no. 1, pp. 23–28, 2022, doi: 10.11003/JPNT.2022.11.1.23.

[28] S. Seo, P.-W. Son, Y. Han, S.-H. Park, and J.-C. Lee, "Design of performance monitoring system for eLoran time synchronization service," *J. Korean Soc. Mar. Environ. Saf.*, vol. 27, no. 6, pp. 815–821, Oct. 2021, doi: 10.7837/kosomes.2021.27.6.815.

[29] P.-W. Son, S. Lee, T. H. Fang, and K. Seo, "Analysis of LDC message reception performance of Korean eLoran pilot service according to modulation methods," *J. Navigat. Port Res.*, vol. 46, no. 6, pp. 525–529, 2022, doi: 10.5394/KINPR.2022.46.6.525.

[30] *Specification of the Transmitted Loran-C Signal*, Standard COMDTINST M16562.4, USCG, 1994.

[31] *Transmitted Enhanced Loran (eLoran) Signal Standard*, Standard SAE9990, SAE Int., Warrendale, PA, USA, 2018.

[32] *Loran-C User's Handbook*, U.S. Government Printing Office, Washington, DC, USA, 1992.

[33] *Minimum Performance Standards for Marine eLoran Receiving Equipment*, Standard RTCM SC-127, RTCM, 2017.

[34] S. Lo, M. Leathem, G. Offermans, G. Gunther, B. Peterson, G. Johnson, and P. Enge, "Defining primary, secondary, additional secondary factors for RTCM minimum performance specifications," in *Proc. 38th Annu. Conv. Tech. Symp. Int. Loran Assoc.*, vol. 1315, Portland, ME, USA, 2009.

[35] I. Astin and Y. Feng, "Technical note: Remote sensing of sea surface salinity using the propagation of low-frequency navigation signals," *Ocean Sci.*, vol. 11, no. 5, pp. 695–698, Sep. 2015, doi: 10.5194/os-11-695-2015.

[36] W. Yan, M. Dong, S. Li, C. Yang, J. Yuan, Z. Hu, and Y. Hua, "An eLoran signal cycle identification method based on joint time–frequency domain," *Remote Sens.*, vol. 14, no. 2, p. 250, Jan. 2022, doi: 10.3390/rs14020250.

[37] S. Li and F. Huang, "Algorithm of cycle-identification for Loran-C signal based on DLL," in *Proc. 8th Int. Conf. Wireless Commun., Netw. Mobile Comput.*, Shanghai, China, Sep. 2012, pp. 1–3, doi: 10.1109/WiCOM.2012.6478390.

[38] A. J. Fisher, "Loran-C cycle identification in hard-limiting receivers," *IEEE Trans. Aerosp. Electron. Syst.*, vol. 36, no. 1, pp. 290–297, Jan. 2000, doi: 10.1109/7.826332.

[39] Y. Gao, Y. Hua, S. Li, and C. Yang, "Acquisition method of Loran-C signal based on matched filter," in *Proc. IEEE Int. Conf. Signal Process., Commun. Comput. (ICSPCC)*, Ningbo, China, Sep. 2015, pp. 1–5, doi: 10.1109/ICSPCC.2015.7338868.

[40] S. C. Lo, B. B. Peterson, and P. K. Enge, "Proving the integrity of the weighted sum squared error (WSSE) Loran cycle confidence algorithm," *Navigation*, vol. 54, no. 4, pp. 277–291, Dec. 2007, doi: 10.1002/j.2161-4296.2007.tb00409.x.

PYO-WOONG SON (Member, IEEE) received the B.S. degree in electrical and electronic engineering from Yonsei University, Seoul, South Korea, in 2012, and the Ph.D. degree in integrated technology from Yonsei University, Incheon, South Korea. He is currently a Senior Researcher with Korea Research Institute of Ships and Ocean Engineering (KRISO) and an Assistant Professor with the University of Science and Technology (UST), Daejeon, South Korea. His research interests include complementary positioning, navigation, and timing systems, such as eLoran. He was a recipient of a Graduate Fellowship from the Information and Communications Technology (ICT) Consilience Creative Program supported by the Ministry of Science and ICT, South Korea.

TAE HYUN FANG (Member, IEEE) received the B.S., M.S., and Ph.D. degrees in mechanical engineering from Pusan National University, Busan, South Korea, in 1994, 1998, and 2003, respectively. From 2004 to 2005, he was a Visiting Scholar with the Intelligent Transportation Research Centre, Massachusetts Institute of Technology, Cambridge, MA, USA. Since 2005, he has been with the Maritime Safety and Environmental Research Division, Korea Research Institute of Ship and Ocean Engineering, Daejeon, South Korea. His research interests include sensor fusion systems, PNT technologies, and target tracking filters.